

Height Tendency Diagnostics Using a Generalized Omega Equation, the Vorticity Equation, and a Nonlinear Balance Equation

JOUNI RÄISÄNEN

Department of Meteorology, University of Helsinki, Helsinki, Finland

(Manuscript received 13 March 1996, in final form 12 November 1996)

ABSTRACT

Height tendency dynamics are studied with a system consisting of a generalized omega equation, the vorticity equation, and a nonlinear balance equation. By using the first two equations, vorticity tendency is first partitioned into components associated with vorticity advection, thermal advection, friction, diabatic heating, and an ageostrophic tendency term. The nonlinear balance equation is then employed to interpret the vorticity tendency components in terms of height tendencies. The height tendencies due to vorticity advection and friction can be divided into parts associated with the direct forcing and the vertical motions induced by this forcing. This division illustrates the efficiency of vertical motions in smoothing out the vertical gradients in the forcing field.

The system is solved over a global domain, but the main emphasis is on an analysis of the "Presidents' Day cyclone" of February 1979. Although the calculations do not fully capture the observed decrease in the deepening rate of this cyclone from 19 to 21 February, they suggest a change in its dynamics. On 19 February thermal advection and diabatic heating due to latent heat release are both found to make a large contribution to intensify the system, on 21 February only the latter makes a contribution. Vorticity advection by the nondivergent flow favors the deepening of the low on both 19 and 21 February, but anticyclonic vorticity advection by low-level convergent winds is identified as a damping mechanism comparable in importance to surface friction. It is also found that the formally passive characteristics of the environment like the stability and vorticity distributions modify the calculated height tendencies rather strongly.

1. Introduction

A characteristic of the atmospheric synoptic-scale dynamics is that vertical motions are more naturally thought as a slave of other processes than as an independent forcing agent. According to the quasigeostrophic (QG) theory (e.g., Holton 1992), the vertical circulation is such that it just compensates the tendency of vorticity advection and thermal advection to remove the atmosphere from geostrophic and hydrostatic balance. One implication of this is that the vorticity equation, when used alone, is a somewhat problematic tool for analyzing the dynamics of synoptic systems. For example, if one wishes to use this equation to study the role of vorticity advection in a given case, one can of course directly calculate this term. But the stretching term may be equally important, and since vorticity advection affects the vertical circulation, some part of this term is likely to present an indirect effect of vorticity advection. Moreover, since the vertical circulation is affected by other processes as well (in the QG theory, thermal advection), this part is not readily separable.

Similar problems are encountered in using the thermodynamic equation alone.

Within the QG framework, problems like those discussed above can of course be avoided by using a diagnostic tool that combines the vorticity and the thermodynamic equation: the QG height tendency equation (Holton 1992, 159). In many cases, however, the numerous approximations in the QG theory itself hamper the usefulness of this tool; it is not always able to reproduce the actual height tendencies with an acceptable accuracy. To overcome this problem, Tsou et al. (1987) derived a generalized height tendency equation and demonstrated that this was far superior to the QG equation in reproducing the observed height tendencies. In this equation, however, vertical motions are not as neatly eliminated as in the QG counterpart. One of the major forcing terms is vertical stability advection, and, as found by Tsou et al. and in a few later studies (e.g., Tsou and Smith 1990; Tan and Curry 1993), this term has a strong tendency to oppose the other large terms.

In this paper, an alternative method to height tendency diagnostics is presented. While this method makes few approximations to the primitive equations and hence is expected to be accurate even in cases in which the QG approximations break down, it also formally eliminates vertical motions as an independent forcing mechanism. To achieve this elimination, a generalized omega equa-

Corresponding author address: Jouni Räisänen, Department of Meteorology, University of Helsinki, P.O. Box 4 (Yliopistonkatu 3), FIN-00014 Helsinki, Finland.
E-mail: Jouni.Raisanen@Helsinki.Fi

tion is first used. Then the solution of this equation is substituted to the vorticity equation to obtain a partitioning of the vorticity tendency. Finally, a nonlinear balance equation is used to interpret the calculated vorticity tendencies in terms of height tendencies.

After presenting the equation system in more detail (section 2), the database and the numerical methods are described in section 3. The system is solved over a global domain, hence a few brief remarks of the planetary-scale behavior of the calculated height tendencies are given in section 4. However, the emphasis in this study is on an analysis of the so-called Presidents' Day

cyclone over the western North Atlantic on 19–21 February 1979 (section 5). In addition to presenting the calculated height tendencies, various aspects of their physical interpretation are discussed, including, for example, the “direct” and “indirect” effects of vorticity advection and friction. A summary followed by some further discussion is given in section 6.

2. Equations

The starting point of the present analysis is the generalized omega equation in the form used by Räisänen (1995, hereafter R95):

$$\begin{aligned} \nabla^2(\sigma\omega) + f\frac{\partial}{\partial p}\left[(\zeta + f)\frac{\partial\omega}{\partial p}\right] - f\frac{\partial}{\partial p}\left(\frac{\partial\zeta}{\partial p}\omega\right) + f\frac{\partial}{\partial p}\left[\mathbf{k}\cdot\left(\frac{\partial\mathbf{V}}{\partial p}\times\nabla\omega\right)\right] \\ = \underbrace{f\frac{\partial}{\partial p}[\mathbf{V}\cdot\nabla(\zeta + f)]}_{F_v} + \underbrace{\frac{R}{p}\nabla^2(\mathbf{V}\cdot\nabla T)}_{F_T} - \underbrace{f\frac{\partial}{\partial p}(\mathbf{k}\cdot\nabla\times\mathbf{F})}_{F_F} - \underbrace{\frac{R}{C_p p}\nabla^2 Q}_{F_Q} + \underbrace{\left[f\frac{\partial}{\partial p}\left(\frac{\partial\zeta}{\partial t}\right) + \frac{R}{p}\nabla^2\frac{\partial T}{\partial t}\right]}_{F_A}, \end{aligned} \quad (1)$$

where all the symbols have their usual meteorological meaning (e.g., Holton 1992). On the right-hand side (rhs), the first four forcing terms represent the effects of vorticity advection, thermal advection, friction, and diabatic heating. The F_A term is at extratropical latitudes closely proportional to the pressure derivative of the ageostrophic vorticity tendency (see R95) and will in the following be referred to as the ageostrophic tendency term. Since the left-hand side (lhs) of (1) is linear with respect to ω , the contributions of the five rhs terms can be calculated separately provided that homogeneous boundary conditions ($\omega = 0$ at the boundaries) are used. By doing this and then using the vorticity equation

$$\begin{aligned} \frac{\partial\zeta}{\partial t} = -\mathbf{V}\cdot\nabla(\zeta + f) - \omega\frac{\partial\zeta}{\partial p} + (\zeta + f)\frac{\partial\omega}{\partial p} \\ + \mathbf{k}\cdot\left(\frac{\partial\mathbf{V}}{\partial p}\times\nabla\omega\right) + \mathbf{k}\cdot\nabla\times\mathbf{F}, \end{aligned} \quad (2)$$

five components of vorticity tendency are obtained:

$$\frac{\partial\zeta}{\partial t} = \left(\frac{\partial\zeta}{\partial t}\right)_v + \left(\frac{\partial\zeta}{\partial t}\right)_T + \left(\frac{\partial\zeta}{\partial t}\right)_F + \left(\frac{\partial\zeta}{\partial t}\right)_Q + \left(\frac{\partial\zeta}{\partial t}\right)_A, \quad (3)$$

where the subscripts follow the convention in (1). These components are defined as

$$\begin{aligned} \left(\frac{\partial\zeta}{\partial t}\right)_v = -\mathbf{V}\cdot\nabla(\zeta + f) - \omega_v\frac{\partial\zeta}{\partial p} + (\zeta + f)\frac{\partial\omega_v}{\partial p} \\ + \mathbf{k}\cdot\left(\frac{\partial\mathbf{V}}{\partial p}\times\nabla\omega_v\right), \end{aligned} \quad (4)$$

$$\begin{aligned} \left(\frac{\partial\zeta}{\partial t}\right)_F = \mathbf{k}\cdot\nabla\times\mathbf{F} - \omega_F\frac{\partial\zeta}{\partial p} + (\zeta + f)\frac{\partial\omega_F}{\partial p} \\ + \mathbf{k}\cdot\left(\frac{\partial\mathbf{V}}{\partial p}\times\nabla\omega_F\right), \end{aligned} \quad (5)$$

and

$$\begin{aligned} \left(\frac{\partial\zeta}{\partial t}\right)_X = -\omega_X\frac{\partial\zeta}{\partial p} + (\zeta + f)\frac{\partial\omega_X}{\partial p} \\ + \mathbf{k}\cdot\left(\frac{\partial\mathbf{V}}{\partial p}\times\nabla\omega_X\right), \quad X = T, Q, A. \end{aligned} \quad (6)$$

Thus, the components associated with vorticity advection and friction include both the vorticity tendencies directly created by these processes and an indirect contribution from the vertical motions induced by them. The other three terms only contain the latter part.

To interpret the vorticity tendencies in terms of height tendencies, we differentiate with respect to time the nonlinear balance equation (NLBE) among the first used by Charney (1955). The result is, in a form that avoids caveats associated with spherical geometry,

$$g\nabla^2 \frac{\partial z}{\partial t} = \nabla \cdot \left(f \nabla \frac{\partial \psi}{\partial t} \right) - \nabla \cdot \left[\nabla \left(\nabla \psi \cdot \nabla \frac{\partial \psi}{\partial t} \right) - \left(\nabla^2 \psi \nabla \frac{\partial \psi}{\partial t} + \nabla \psi \nabla^2 \frac{\partial \psi}{\partial t} \right) \right], \quad (7)$$

where the streamfunction ψ fulfills the relationship

$$\nabla^2 \psi = \zeta. \quad (8)$$

By first converting the calculated vorticity tendency components in (3) into streamfunction tendencies with (8) and then substituting these together with the current streamfunction ψ to (7), five height tendency components are obtained:

$$\frac{\partial z}{\partial t} = \left(\frac{\partial z}{\partial t} \right)_V + \left(\frac{\partial z}{\partial t} \right)_T + \left(\frac{\partial z}{\partial t} \right)_F + \left(\frac{\partial z}{\partial t} \right)_Q + \left(\frac{\partial z}{\partial t} \right)_A. \quad (9)$$

The conversion from (3) to (9) is straightforward apart from the fact that (7) only gives the horizontal Laplacian of $\partial z/\partial t$, not $\partial z/\partial t$ itself. In the present case, in which a global calculation domain is used, the five components in (9) are most simply determined by assuming that the global average is zero for each of them. If the domain were smaller, lateral boundary conditions would have to be specified.

In spite of the relative completeness of the system (1)–(9) compared with diagnostic systems based, for example, on the QG equations, at least two sources of inherent inaccuracy are worth noting. First, while (1) requires only hydrostatic balance, the lower boundary condition $\omega = 0$ used in solving it is not adequate in mountainous areas where near-surface vertical motions may be significant. To account for this, an extra ω component associated with the lower boundary condition should actually be included. As was done by R95, however, this term is excluded in the present study as one too difficult to estimate. In the case of the marine cyclone that is our major focus, this is not expected to be a serious source of error. At any event, boundary conditions would be a more serious issue if the QG or the Tsou et al. (1987) height tendency equation were used since a simple prespecification of $\partial z/\partial t$ at the lower and upper boundaries would be a rather problematic step.

Second, the NLBE is not an exact relationship, even though the approximations in it are for most purposes regarded as small (e.g., Haltiner and Williams 1980, 69) and the nonlinear balance has been shown to explain an appreciable part of the total ageostrophic wind in cyclogenesis events as extreme as the IOP 4 case (Davis et al. 1996). The extent to which the inaccuracy of the NLBE affected the present calculations is discussed in section 5b. Although this impact was not found totally negligible, it clearly appeared acceptably small. In any case, it is fair to note that this source of inaccuracy is in a way unnecessary since the use of the NLBE could

have been avoided by portraying the results in terms of vorticity or streamfunction (rather than height) tendencies. However, vorticity tendencies have the disadvantage of emphasizing subsynoptic features that may be sensitive to numerical errors in the calculations. In addition, although this is partly a matter of personal preference, geopotential height may be regarded as a more natural indicator of cyclone development than the streamfunction simply because it is, unlike the streamfunction, a locally measurable quantity.

A few other issues related to the system (1)–(9) also deserve attention. First, although the use of the generalized omega equation has allowed us to build a system in which the influence of vertical motions is implicitly accounted for, it is evident that some of the five forcing terms in this equation are affected by vertical motions themselves. An obvious example is diabatic heating. A major component of this is latent heat release, which at least in areas of stable ascent tends to be proportional to the intensity of the synoptic-scale rising motion. In addition, vorticity advection (which also enters the system directly via the vorticity equation) and thermal advection contain contributions by the horizontal divergent circulation, which is related to the field of vertical motions by the requirement of mass continuation. Although scaling arguments typical to those used in text books of dynamic meteorology (e.g., Holton 1992) indicate that vorticity advection and thermal advection by divergent wind are of minor importance in most synoptic-scale systems, it is demonstrated in section 5f of this paper that the former of these may actually play a rather large role in some circumstances.

Second, although this is more a formal than a physically meaningful partitioning, it is in the case of vorticity advection and friction instructive to compute separately the height tendencies associated with the direct and the indirect forcing. Examples of such calculations will be shown in section 5e.

Third, the height tendency response to a given forcing is in the system (1)–(9) not solely determined by the forcing itself. Rather, it is also affected by the several variable coefficients in these equations that are associated with the wind, vorticity, and stability distributions of the environment. To study this issue, calculations were also made with a simplified equation system in which this variability is largely eliminated (section 5g).

Finally, the goal of formally eliminating the height tendency forcing by vertical motions could be achieved in some other ways as well. After solving the generalized omega equation, one could also proceed, rather than by using the vorticity equation and the NLBE, by integrating the thermodynamic equation vertically like Hirschberg and Fritsch (1991). In this case, the indirect forcing by vertical motions would enter the system via the adiabatic cooling term in the thermodynamic equation. Likewise, the solution of (1) could be used to partition the vertical stability advection term in the Tsou et al. (1987) height tendency equation. While we have

selected in this study to proceed via the vorticity equation, we are not claiming that this approach is a priori better than these other alternatives.

3. Data and numerical methods

Calculations were made at 6-h intervals for a 2-day period beginning at 0000 UTC 19 February 1979. The same dataset generated by ECMWF was used as in R95: initialized FGGE (First GARP Global Experiment) level IIIb “final” analyses for wind, geopotential, and temperature, and model-produced fields of friction and diabatic heating obtained from 2-h forecasts used in the diabatic normal-mode initialization (Wergen 1988). The data were available on a global $1.875^\circ \times 1.875^\circ$ latitude–longitude grid at 19 isobaric levels (initialized analyses) or at 16 hybrid levels (friction and diabatic heating) that in the lower troposphere behave like σ surfaces but in the stratosphere closely approximate isobaric levels (Wergen 1988).

In many phases of the calculations, spherical harmonics were used. A somewhat adverse consequence of this numerically practical choice was that, at each isobaric level down to the lowest (1000 mb), the grid points below the ground had to be used in the calculations as well as those above the ground. This creates a problem since the calculated height tendency at any given point is not solely determined by the local forcing. The inverse Laplacian in converting $\partial\zeta/\partial t$ to $\partial\psi/\partial t$ spreads the impact of the local vorticity tendency horizontally to all the other grid points at the same isobaric level, and because of the vertical derivatives on the lhs of (1), the vorticity tendencies themselves feel the rhs forcing in all grid points not only at the same but also at the other levels. Thus, even above the ground, the solution may be sensitive to the artificial below-ground input data. In some cases, this sensitivity was actually quite strong, in particular at the planetary scale (see section 4). To minimize the problem, vorticity advection, thermal advection, and diabatic heating were set to zero below the ground. For friction, a slightly different scheme was selected: the interpolation from hybrid levels to isobaric coordinates was made by assuming a constant surface pressure of 1000 mb. While this scheme locates the friction layer in mountainous areas far below the actual surface, it ensures that the strongest friction just above the surface is not lost and that the thickness of the friction layer is always approximately correct.

Another point worth noting is that the 6-h time interval of the FGGE analyses prohibited the calculation of truly instantaneous values for the ageostrophic tendency term $(\partial z/\partial t)_A$. Therefore, we only show in section 5 (Figs. 6e, 7e, 8e, and 9e) an estimate of the 6-h height changes associated with this term. For this estimate, the vorticity and temperature tendencies were replaced with 6-h finite differences between two successive analyses. Then, as the system (1), (6), and (7) contains several variable coefficients, this system was solved twice: first

with coefficients representative for the beginning of the 6-h period and then with coefficients representative for the end of this period. Finally, the two different height tendencies obtained in this way were averaged. However, while this kind of a procedure gives the best available estimate of the magnitude of $(\partial z/\partial t)_A$, these 6-h estimates are necessarily somewhat out of phase with the other “instantaneous” terms. Therefore, the contribution of this term to the total height tendencies shown in Figs. 6f, 7f, 8f, 9f, and 14a,b was calculated from the mean of the height changes computed for the preceding and the following 6 h.

The method used to solve the generalized omega equation is described by R95. Here ω was computed for 20 evenly spaced isobaric levels (50, 100, . . . , 1000 mb). The partitioned vorticity tendencies were then calculated for the 19 half-levels (75, 125, . . . , 975 mb) of this grid. These levels were used in all the subsequent calculations, and for comparison with the calculated height changes, the analyzed height changes were also interpolated onto them. This seemingly unobvious choice, which was ultimately dictated by a technical detail¹ in solving the omega equation, was basically motivated by the need of good numerical consistency between the methods used in solving the vorticity equation and the omega equation. Badly selected methods were found to cause a disturbing amount of vertical noise in $(\partial z/\partial t)_V$ and $(\partial z/\partial t)_F$, which are numerically the most problematic of the five components since they contain two generally opposing parts (see section 5e): the direct contributions of vorticity advection and friction and the indirect contributions from the associated vertical motion. While the details of the methodology are here subordinate to the topic, it is good to note that the vertical interpolations were made, to the extent possible, in the last phase of the computations. For example, in both the omega and the vorticity equations, vorticity advection was fully evaluated at the original FGGE levels before any vertical interpolation. In all these computations, the horizontal derivatives were estimated with fourth-order central differences.

The streamfunction tendencies were obtained from the vorticity tendencies by inverting the horizontal Laplacian with the help of spherical harmonics (e.g., Holton 1992, 452). The expansions were truncated at the two-dimensional wavenumber $n = 63$. The current streamfunction was calculated from the FGGE wind analysis in the same way. Finally, the height tendency components were solved from (7) by first evaluating the

¹ In the core of solving (1), a matrix inversion was used in which $\partial^2\omega/\partial p^2$ was directly approximated with the traditional three-point formula on the 20-level grid. To get the pressure derivative of $\partial\zeta/\partial t$ consistent with this scheme, $\partial\omega/\partial p$ had to be estimated in the vorticity equation at the half-levels of the 20-level grid from the difference of ω between two adjacent full levels.

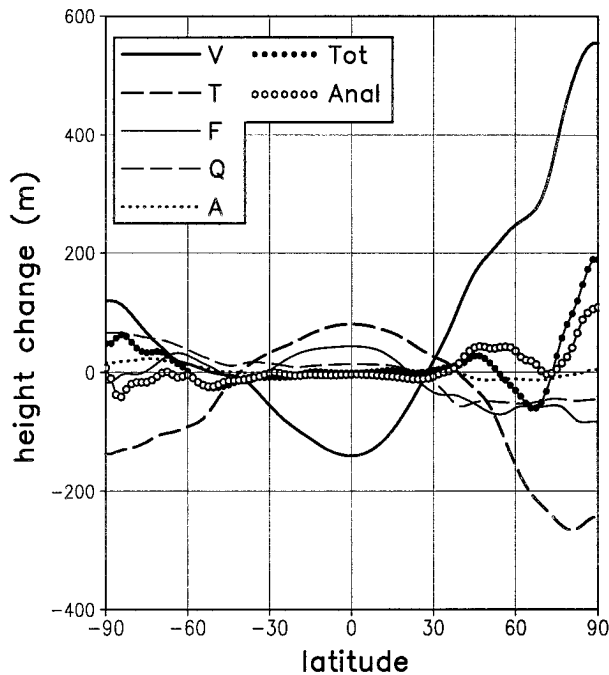


FIG. 1. The 48-h (0000 UTC 19 February–0000 UTC 21 February 1979) zonal mean changes in the 925-mb isobaric height associated with the five terms of Eq. (9) (V , T , F , Q , and A). The total calculated (Tot) and analyzed (Anal) zonal mean height changes are also shown.

rhs in grid space and then inverting the Laplacian with spherical harmonics.

4. Planetary-scale characteristics

To briefly characterize the planetary-scale behavior of the calculated height tendencies, Fig. 1 shows for the 925-mb level the 48-h zonal mean height changes associated with the five terms in (9). The zonal means of the calculated total height changes and the analyzed height changes are also included. The 925-mb level is selected here since it is most heavily used in the rest of the paper. However, most of the terms in (9) had a relatively barotropic structure in the zonal mean plane, in particular in the lower and midtroposphere.

The purpose of showing Fig. 1 is not to discuss the planetary-scale height tendency dynamics in any detail; for this aim the 48-h averaging period is in fact spuriously short. Rather, this figure serves to illustrate a feature that for any synoptic-scale analysis must be regarded as a nuisance. Two of the five components, $(\partial z/\partial t)_V$ and $(\partial z/\partial t)_T$, have in the zonal mean plane a rather large magnitude [the former exceeds $500 \text{ m (48 h)}^{-1}$ near the North Pole] and a strong tendency to oppose each other. In the Tropics and the polar regions, the zonal means shown in Fig. 1 are in fact comparable to, or larger than, the transient features of $(\partial z/\partial t)_V$ and $(\partial z/\partial t)_T$ in typical synoptic systems. Consequently, even though the Presidents' Day storm was a strong midla-

titude cyclone, it was found useful to simplify the synoptic interpretation by removing the very longest wave components (two-dimensional wavenumber $n \leq 3$) from all the calculated height tendencies (but not from the analyzed height changes) shown in section 5. In addition to just discussing the contributions of $(\partial z/\partial t)_V$ and $(\partial z/\partial t)_T$, this long-wave cutoff clearly appeared beneficial in a few other issues, for example in analyzing the direct and indirect effects of vorticity advection (section 5e).

The removal of the longest waves is justified by the fact that these waves had, with the exception of the stratosphere, a relatively small amplitude in the analyzed height change field. The global maximum of their 48-h contribution at 925 mb was only 60 m. Moreover, although the smallness of this contribution does not strictly rule out the possibility that *some* synoptically relevant information has been thrown away, the situation is loosely analogous to the (frequent) case in which calculations are made in a nonglobal domain. Even in that case, the planetary-scale tendencies would not be properly presented. Finally, it is to be emphasized that the long-wave cutoff was only made after fully solving the system (1)–(9). Therefore, the results shown in section 5 appropriately include the synoptic-scale ($n > 3$) height tendencies resulting from the nonlinear interactions in which the planetary-scale waves are involved.

Figure 1 also reveals that the total calculated 48-h height changes were not identical with the analyzed height changes: zonal mean differences approaching $100 \text{ m (48 h)}^{-1}$ occur in high latitudes. While the causes of the errors are not fully known, it is speculated that the treatment of the below-ground input data may play some role, in spite of the countermeasures described in the previous section. Without these countermeasures, the results were clearly more unrealistic. For example, when vorticity advection was not set to zero below the ground, $(\partial z/\partial t)_V$ was over $150 \text{ m (48 h)}^{-1}$ more positive at the North Pole, and over $350 \text{ m (48 h)}^{-1}$ more positive at the South Pole.

5. Analysis of the Presidents' Day cyclone

a. Overview of the synoptic development

The vigorous depression known as the Presidents' Day cyclone developed when an inverted trough situated at the east coast of the United States on 18 February 1979 underwent a period of rapid deepening on the following day. This case of explosive cyclogenesis has been widely studied by using both observational data (e.g., Bosart 1981; Bosart and Lin 1984; Uccellini et al. 1984, 1985) and model simulations (Uccellini et al. 1987; Whitaker et al. 1988); therefore, no detailed description of the synoptic development is needed here. However, since our calculations extend later in time than those in these earlier studies, the track of the surface low and the evolution of its minimum sea level pressure

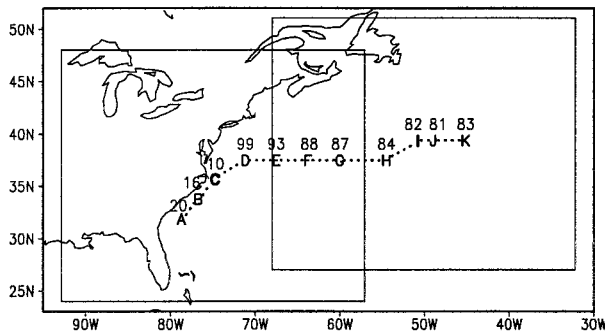


FIG. 2. Position and minimum SLP of the surface low as a function of time. The letters A–K give the position at 6-h intervals (A—0000 UTC 19 February, . . . , C—1200 UTC 19 February, . . . , I—0000 UTC 21 February, . . . , K—1200 UTC 21 February 1979) and the figures the SLP in millibars with full hundreds omitted. The two rectangles show the domains used in portraying the results for 1200 UTC 19 February and 0000 UTC 21 February, respectively.

(SLP) until 1200/21² are shown in Fig. 2. In accord with Bosart (1981), the FGGE analyses used here place the most rapid deepening of the low between 1200 and 1800/19. After this, a slower deepening continued until 0600/21. During the period for which comparison is possible, the SLP values shown in Fig. 2 are somewhat higher than those reported by Bosart (1981), but this is at least partly due to the relatively coarse horizontal resolution of the FGGE analyses.

The earlier studies (e.g., Bosart 1981; Bosart and Lin 1984; Uccellini et al. 1985) show that the explosive cyclogenesis on 19 February was triggered by the approach of an eastward-moving polar jet–trough system. However, an equally necessary ingredient was the initial lower-tropospheric trough, the evolution of which had been favored by strong low-level baroclinity (Bosart 1981), large fluxes of sensible and latent heat (Bosart and Lin 1984), and upper-level divergence associated with a subtropical jet streak (Uccellini et al. 1984). As witnessed by the heavy snowfall (e.g., Bosart 1981; Whitaker et al. 1988) observed already on 18 February but more markedly on 19 February, substantial latent heat release also took place. In addition, Uccellini et al. (1987) and Whitaker et al. (1988) point out that the various diabatic and adiabatic processes appeared to interact in a synergistic, mutually beneficial manner. Such a synergy between different processes may in fact pose difficulties in attempts to separate their individual contributions. While the method developed in section 2 is expected to give a lot of information on the instantaneous height tendency dynamics, it is necessarily unable to track the indirect effects that may become important in course of time. In spite of this restriction, the Presidents' Day cyclone is a most interesting case for the application of this method.

² 1200/21 means 1200 UTC 21 February.

Although the computations (apart from those reported in section 5g) were made at 6-h intervals, the following analysis will concentrate on two synoptic times: 1200/19, which just precedes the largest observed 6-h deepening, and 0000/21, when the cyclone had virtually reached its minimum SLP. In all their main respects, the diagnostics obtained at 1200/19 and 0000/21 appeared to be representative of the rapid deepening stage and the mature stage of the cyclone, respectively.

Some aspects of the synoptic situation at 1200/19 and 0000/21 are shown in Fig. 3. At 1200/19, a sharp upper-tropospheric trough with strong positive vorticity advection ahead was approaching from the west (Fig. 3a). This trough and the associated vorticity maximum were still visible but less pronounced at 0000/21 (Fig. 3b). By contrast, the surface low grew much more vigorous from 1200/19 to 0000/21 (Figs. 3c,d); at the latter time, the absolute vorticity locally exceeded $4 \times 10^{-4} \text{ s}^{-1}$ near 900 mb. At both 1200/19 and 0000/21, the environment of the low was characterized by very strong lower-tropospheric baroclinity. On the eastern and northern sides of the low, precipitation was accompanied by condensation heating, which according to the ECMWF heating fields reached at 1200/19 a peak value of 2.5 K h^{-1} . At 0000/21, the model-estimated mid-tropospheric diabatic heating was even stronger, the maximum being over 4 K h^{-1} .

b. Comparison of calculated and analyzed height tendencies

In this section, the calculated and analyzed height changes are compared. Since no “instantaneous” analyzed height tendencies were available, the comparison was made on a 6-h basis: for each of the eight 6-h periods from 0000–0600/19 to 1800/20–0000/21, the calculated height tendencies at the beginning and the end of the period were averaged, and this average was compared with the analyzed 6-h changes. To estimate how the use of the NLBE affected the results, the comparison also included the 6-h height changes obtained by directly applying the NLBE to the vorticity fields inferred from the wind analyses. For each 6-h period, two kinds of statistics were computed for a 24° latitude \times 36° longitude box around the center of the surface low: the root-mean-square (rms) amplitudes [i.e., the square roots of the area mean of $(\partial z/\partial t)^2$] for all the three fields, and the spatial correlation between the other two fields and the analyzed height changes.

The statistics averaged over the eight periods are shown in Fig. 4. In general, they indicate a moderately good agreement between the calculated and analyzed height changes. The mean correlation between these, shown by the solid line in Fig. 4a, exceeds 0.8 at all levels below 250 mb and 0.9 in the lower troposphere. The correlation at the few uppermost levels is much lower, but these levels are of a secondary interest for the present study. In addition, as seen from the rms

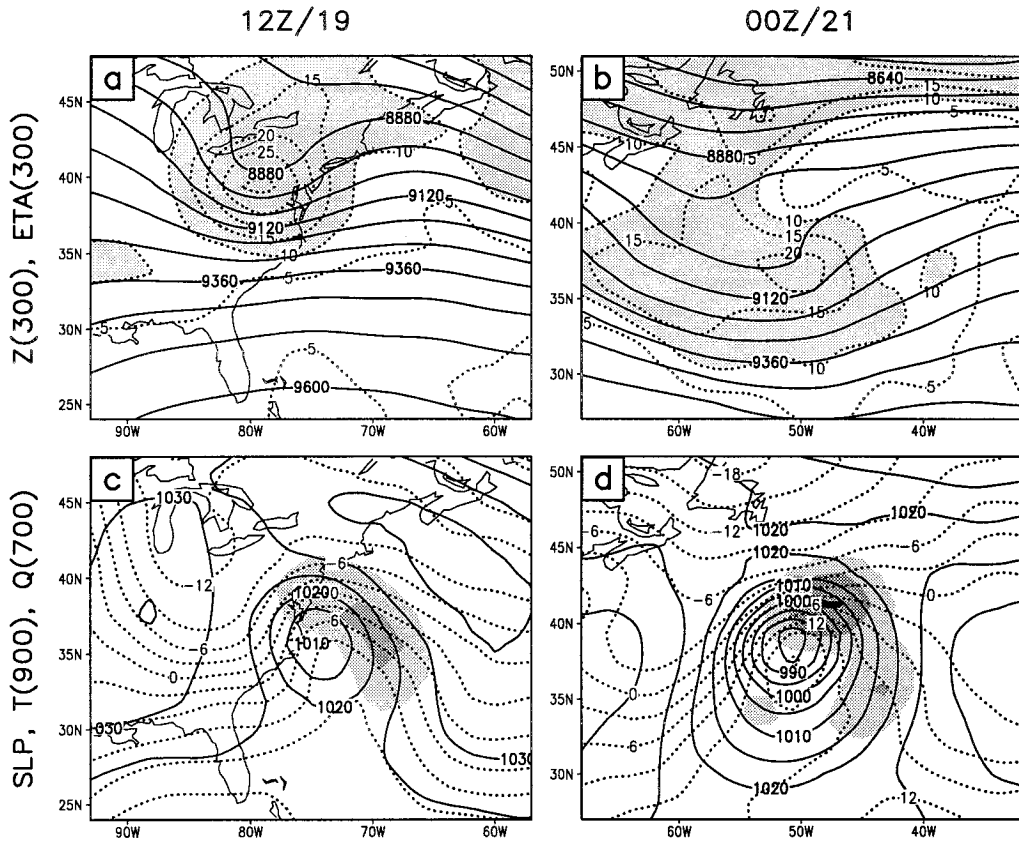


FIG. 3. Synoptic situation at 1200 UTC 19 February [(a) and (c)], and 0000 UTC 21 February [(b) and (d)]. Panels (a) and (b) depict geopotential height (solid, every 80 m) and absolute vorticity in 10^{-5} s^{-1} (dotted, every $5 \times 10^{-5} \text{ s}^{-1}$, values in excess $10 \times 10^{-5} \text{ s}^{-1}$ shaded) at 300 mb. In (c) and (d), sea level pressure (solid, every 5 mb), temperature at 900 mb (dotted, every 3°C) and diabatic heating at 700 mb are shown. The light, medium, and dark shading indicate heating rates of 0.5–2, 2–4, and over 4 K h^{-1} , respectively.

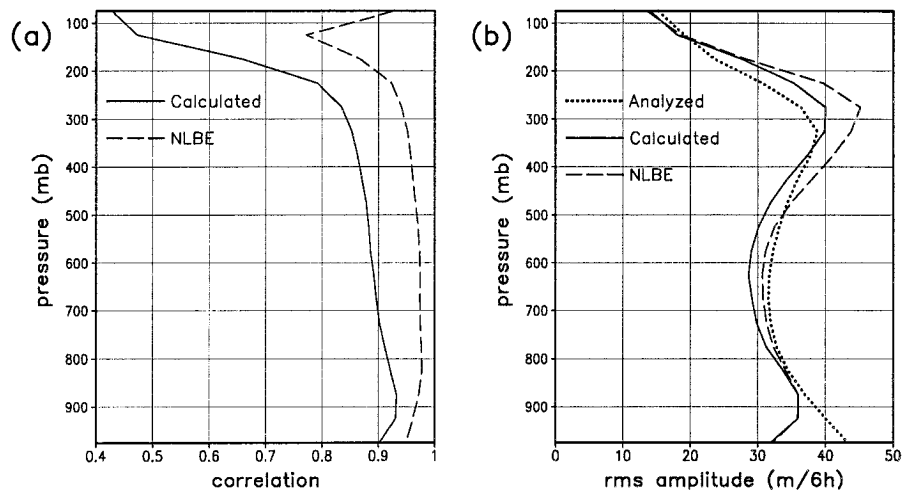


FIG. 4. (a) Time mean spatial correlation in the vicinity of the cyclone (see text) between the analyzed and the calculated 6-h height changes (solid) and between the analyzed height changes and the height changes estimated with the NLBE directly from the wind analyses (dashed). (b) The rms amplitudes for the analyzed (dotted) and calculated (solid) height changes and for the height changes estimated with the NLBE from the wind analyses (dashed).

amplitudes in Fig. 4b, the height changes at this altitude were relatively small. The rms amplitudes for the calculated and analyzed height changes are in fair agreement, although some differences are easily detectable. Most notably, the calculated height changes at the lowest level, 975 mb, are too weak by over 25%.

The relative weakness of the calculated low-level height changes is consistent with the fact that the NLBE neglects surface friction and therefore does not “know” that a steeper pressure gradient is needed to maintain a given wind speed near the surface than in the free atmosphere. Thus, low-level vorticity tendencies of the right magnitude should lead to too small inferred height tendencies. As seen from Fig. 4b, a very similar error in the low-level rms amplitude was actually found in the test in which the NLBE was directly applied to the wind analyses. This test also revealed that the NLBE tended to overestimate the magnitude of the analyzed height changes in the upper troposphere and the lowermost stratosphere, but this positive bias is more difficult to explain. In any case, the fields obtained in this test were spatially highly correlated with the analyzed height changes, in particular in the troposphere: the mean correlation exceeded 0.95 at all levels below 300 mb and approached 0.98 near 800 mb (see the dashed line in Fig. 4a). As a whole, therefore, the inaccuracy of the NLBE seems for the purposes of the present study an acceptable source of error.

In sections 5c–g, all the horizontal height tendency fields are shown at the 925-mb level, which partly avoids the friction-related inaccuracy of the NLBE near the surface but still appeared low enough to give a representative view of the factors that affected the development of the low-level cyclone. Figure 5 shows height changes at this level during 1200–1800/19 and 1800/20–0000/21, that is, for the 6-h periods following the first and preceding the second synoptic time on which the rest of our analysis will concentrate. The analyzed height changes, the height changes obtained by averaging the calculated total height tendencies at the beginning and the end of the period, and the height changes inferred from the wind analyses with the NLBE are all shown. During both periods, the areas of height decrease and increase in these three fields are nearly collocated. Another common feature is the general increase in the magnitude of the height changes from 1200–1800/19 to 1800/20–0000/21, which is explained by the movement of the cyclone together with the larger intensity of the surface low during the latter period.

In the details, however, differences do emerge between the three fields. Compared with the analyzed height changes (Figs. 5a,b), the calculated height changes (Figs. 5c,d) have at both times a less concentrated spatial structure and a smaller maximum magnitude. Although several factors may contribute to this, the presence of a similar though less pronounced error in the height change fields inferred with the NLBE directly from the wind analyses (Figs. 5e,f) is worth not-

ing. The general deficit in magnitude is at least partly due to friction, but friction alone is unlikely to explain the looser spatial structure near the center of the low. This might either indicate that the flow near the core of the cyclone was actually unbalanced, or simply result from numerical smoothing of small-scale details in the calculations.

Perhaps the most disappointing conclusion from comparing Figs. 5c,d with 5a,b is that the calculated height changes do not properly capture the marked decrease in the deepening rate of the cyclone from 1200–1800/19 to 1800/20–0000/21. During the former period, the calculations underestimate the height decrease ahead of the low more severely than the height increase behind the low, but during the latter, the height increase is more seriously underestimated³. The calculated height tendency at the center grid point of the low actually appears to be more strongly negative during 1800/20–0000/21 than 1200–1800/19, but this impression may be somewhat misleading. Although the height tendency at the center of the low is in principle the best measure of the deepening rate, this measure is not quantitatively very useful when one can only determine the position of the low center with an accuracy of roughly 200 km, in particular as the height tendency gradient near the center of the low is very large.

Despite the problem just noted, a further analysis is motivated by the fact that appreciable changes from the period of the observed rapid deepening to the mature stage of the cyclone were found in some of the individual terms in (9). From here on, the calculated height tendencies will for simplicity be displayed as instantaneous fields rather than as 6-h averages, apart from $(\partial z/\partial t)_A$ for which this was not possible. However, the units meters per 6 hours will still be used.

c. Contributions of individual terms at 1200 UTC 19 February

The individual contributions of the five terms in (9) to the 925-mb height tendencies at 1200/19 [or, in the case of $(\partial z/\partial t)_A$, between 1200/19 and 1800/19] are shown in Figs. 6a–e. Figure 6f displays the calculated total height tendency, which is slightly different from that shown in Fig. 5c since averaging over two analysis times is not used. Vorticity advection (Fig. 6a) and thermal advection (Fig. 6b) both induce a negative height tendency on the eastern or northeastern side of the surface low and a positive height tendency on the opposite side. Thus, they are important for the movement of the cyclone. However, the negative height tendency induced by thermal advection extends well over the low center and is several times larger than the positive height ten-

³ As noted in section 4, the calculated height change fields shown here exclude the very longest wave components. Even with these waves included, however, the discrepancy was only slightly smaller.

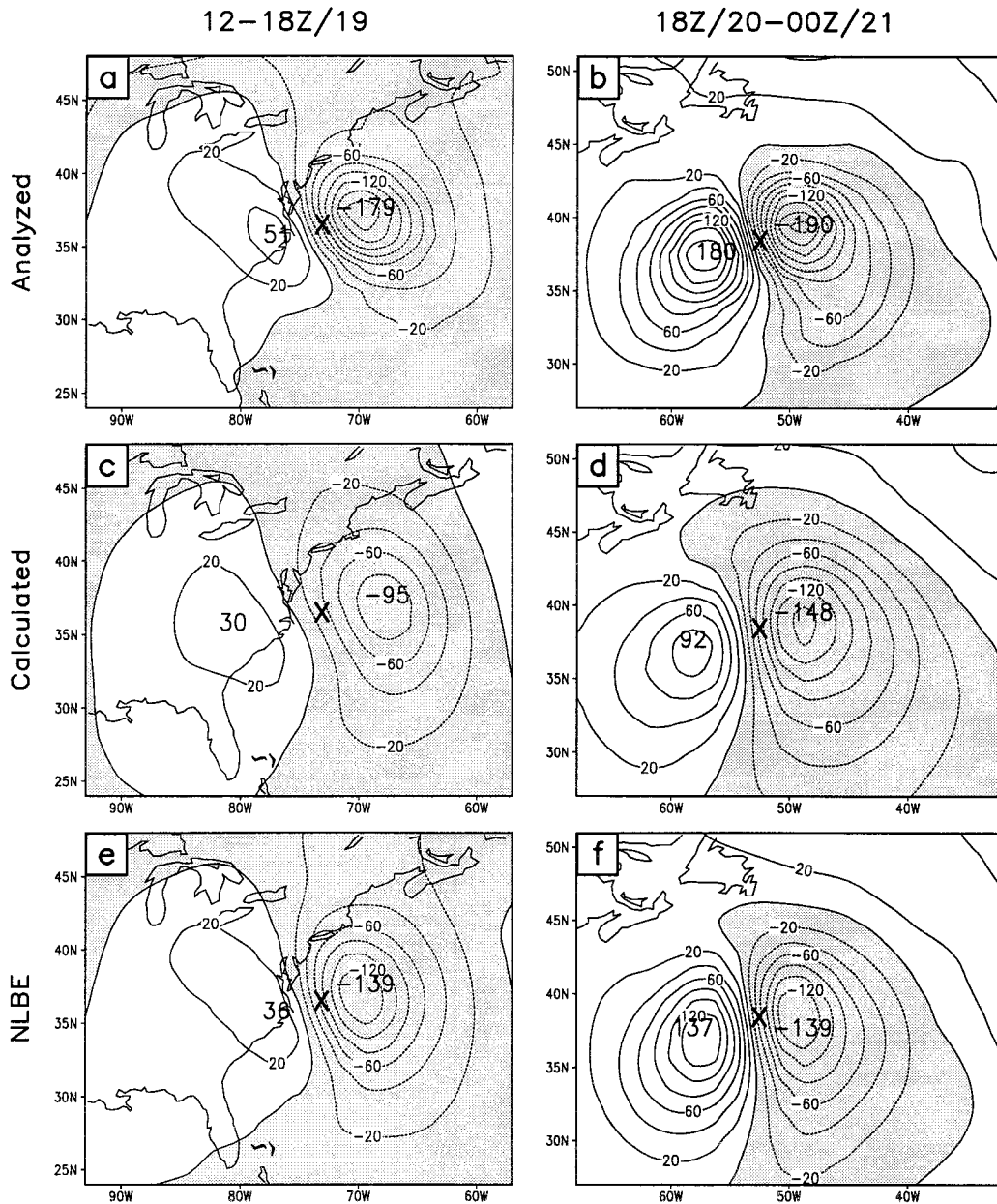


FIG. 5. Height changes at 925 mb from 1200 to 1800 UTC 19 February [(a), (c), and (e)] and from 1800 UTC 20 February to 0000 UTC 21 February [(b), (d), and (f)]. Panels (a) and (b) show the analyzed height changes, (c) and (d) the average of the calculated total height tendencies at the beginning and the end of each 6-h period, and (e) and (f) the height changes inferred with the NLBE from the wind analyses. Contour interval is 20 m (6 h)^{-1} ; negative values are shaded. The crosses (X) indicate the estimated position of the surface low at 1500 UTC 19 February and 2100 UTC 20 February 1979.

density behind the low, indicating that this term also plays a substantial role in deepening the low. Vorticity advection also favors the deepening, but much more modestly (as shown in section 5f, this is the net result of two opposing effects). In addition to thermal advection, a major contributor to the deepening is diabatic heating, which induces an extensive area of negative height tendency over and ahead of the surface low (Fig. 6d). Friction

counteracts the deepening by inducing a positive height tendency over the low (Fig. 6c), but the magnitude of this term is fairly small. The ageostrophic tendency term (Fig. 6e) also appears small, even though to some extent this may be affected by the unavailability of the instantaneous vorticity and temperature tendencies. Also note that because of the movement of the cyclone, the field shown in Fig. 6e is somewhat in the

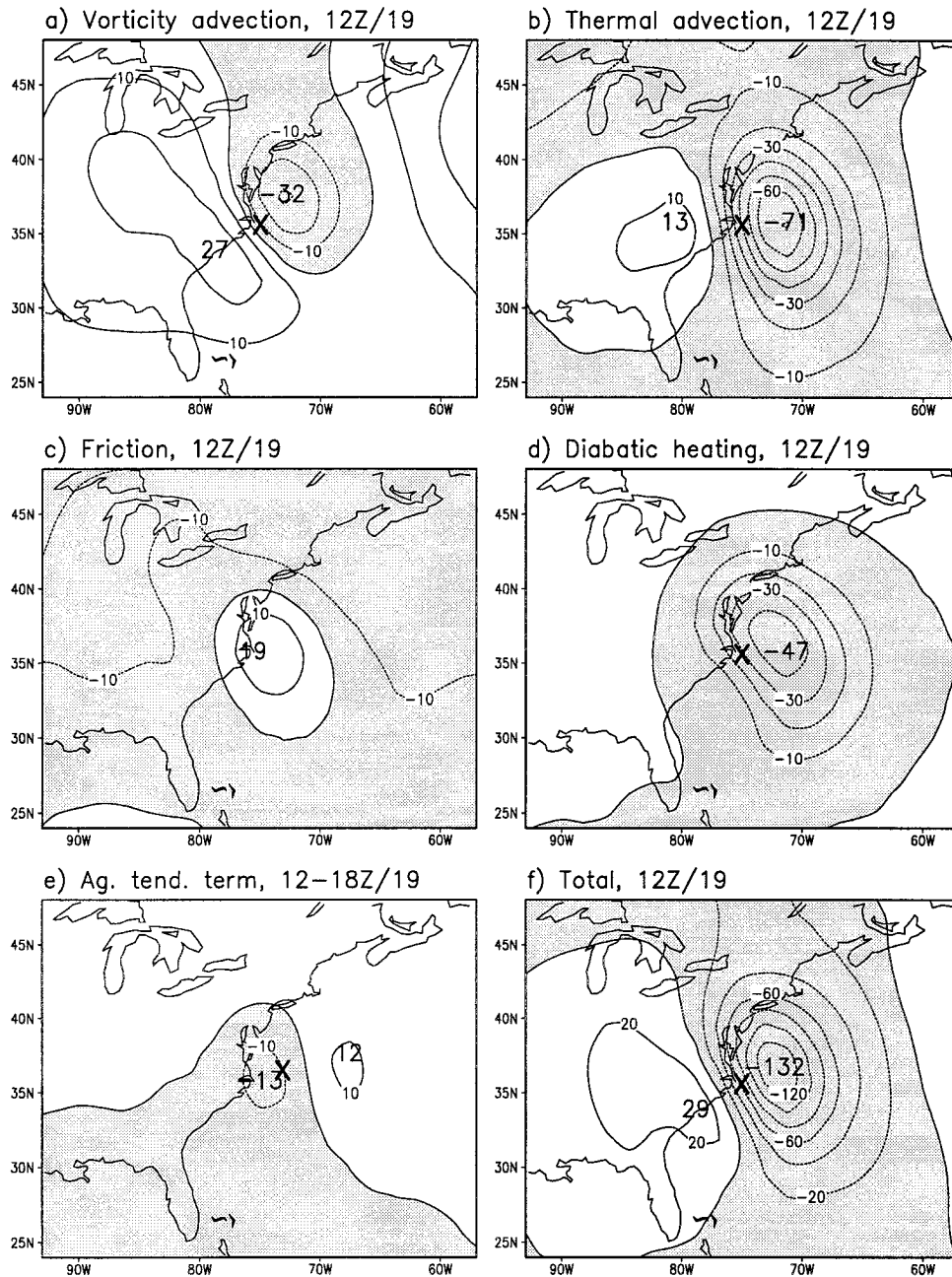


FIG. 6. Contributions to height tendencies at 925 mb at 1200 UTC 19 February: (a) vorticity advection, (b) thermal advection, (c) friction, (d) diabatic heating, and (e) the ageostrophic tendency term (1200–1800 UTC 19 February 1979). The calculated total height tendency is shown in (f). Contour interval is 10 m (6 h)^{-1} in (a)–(e) and 20 m (6 h)^{-1} in (f); negative values are shaded. The cross (X) indicates the position of the surface low.

wrong phase compared with the others. To help the interpretation, the cross indicating the center of the surface low is in Fig. 6e plotted midway between the positions at 1200 and 1800/19 rather than at the position at the former time.

The six fields shown in Fig. 6 are redisplayed in Fig. 7 in east–west-oriented vertical cross sections along

37.5°N (slightly to the north of the surface low). A considerable amount of altitude dependence is seen in all of these fields. Although the contribution of vorticity advection (Fig. 7a) has an equivalent barotropic structure, the negative and positive height tendencies are much larger at the two sides of the upper trough near 300 mb than in the lower troposphere. Thermal advec-

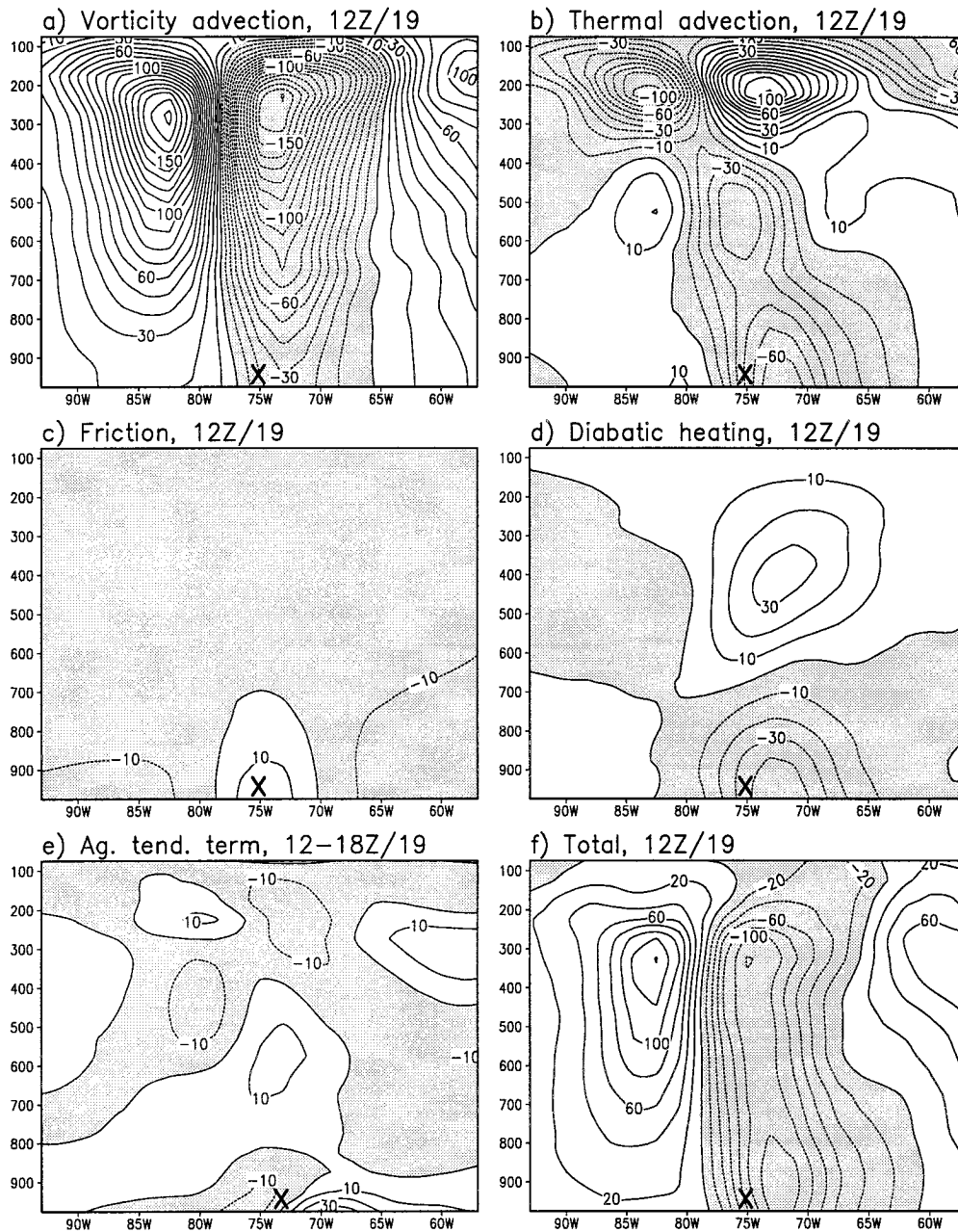


FIG. 7. As Fig. 6 but pressure–longitude cross sections along 37.5°N. The cross (X) indicates the longitude of the surface low.

tion (Fig. 7b) strongly opposes vorticity advection above 350 mb, but it reinforces this to some extent in the midtroposphere. This stratospheric–midtropospheric quadrupole appears somewhat distinct from the cells of negative and (weak) positive height tendency in the lowest troposphere, and as judged from the actual fields of thermal advection, it evidently had its origin in the strong warm and cold advectations at the two sides of the upper trough. Similar to the case analyzed by Hirschberg and Fritsch (1991), the strongest advectations took place between 200 and 400 mb, the warm advection being at

maximum over the developing surface low. The upper-level thermal advectations may have made a contribution to the calculated low-level height tendencies as well, but since areas of strong warm and cold advection also occurred in the lower troposphere, the significance of this contribution remains unknown.

The positive height tendency induced by friction over the surface low is at this time discernible below 700 mb only (Fig. 7c). The negative height tendency above this level is not intuitively expected but is presumably associated with the strong and wide anticyclone that

surrounded the developing but still relatively weak low. A more marked midtropospheric reversal of sign occurs in the contribution of diabatic heating (Fig. 7d); the height decreases in the lower troposphere are accompanied by almost equal height increases around 400 mb. Thus, diabatic heating not only acted to deepen the low-level cyclone but also amplified the western parts of the ridge that preceded the upper trough (compare Fig. 7d with Fig. 3a). This is, in fact, one of the synergistic mechanisms discussed by Uccellini et al. (1987). By shortening the upper wave, diabatic heating indirectly enhanced the positive vorticity advection aloft, which in turn favored the development at lower levels. Finally, the ageostrophic tendency term (Fig. 7e) is largest in the boundary layer; positive values of over 30 m (6 h)^{-1} are found at 975 mb on the eastern side of the surface low. As was the case at other synoptic times, this term tended to oppose the sum effect of the other four in the very lowest troposphere.

d. Contributions of individual terms at 0000 UTC 21 February

The five height tendency components and their sum at 0000/21 are shown in Figs. 8 (horizontal fields at 925 mb) and 9 (vertical cross sections through the center of the surface low at 39.4°N). In addition to a number of similarities, some appreciable differences from the results at 1200/19 are evident. At 925 mb, all five components have now a larger magnitude than 36 h before. The marked asymmetry found in $(\partial z/\partial t)_T$ at 1200/19 has completely vanished (Fig. 8b), while an asymmetry of the opposite sense has emerged in $(\partial z/\partial t)_V$ (Fig. 8a); the height decrease on the eastern side of the low is now significantly smaller than the height increase to the west of the low. These terms have thus both changed in a way that acts to decrease the deepening rate of the low, and this change is reinforced by a marked increase in the positive height tendency induced by surface friction (Fig. 8c). On the other hand, however, the negative height tendency due to diabatic heating has increased substantially to over 110 m (6 h)^{-1} at maximum (Fig. 8d). The ageostrophic tendency term (Fig. 8e) is still the smallest of the five at this level.

The clear dominance of height decreases over height increases in the calculated total height tendency field (Fig. 8f) is somewhat in conflict with the slowness of the analyzed deepening rate of the cyclone and obviously calls for care in considering the results just described. A possible explanation for the discrepancy is that the largeness of the negative $(\partial z/\partial t)_Q$ at this time is not fully realistic. It cannot be ruled out that the model-produced heating fields have been affected, for example, by spinup effects in the 2-h forecasts used to create them. However, it is equally difficult to rule out that $(\partial z/\partial t)_Q$ is actually correct and the problems in the calculated total height tendency stem from some of the other terms.

The strongest negative and positive height tendencies induced by vorticity advection are still found near the tropopause level (Fig. 9a), but a secondary maximum of height increase has developed over the western flank of the surface low in the lower troposphere. The largest height tendencies due to thermal advection are now concentrated in the lowest troposphere (Fig. 9b). In particular, the positive height tendency on the rear side of the low shows a steep vertical gradient below 800 mb, reflecting the strong near-surface cold advection in the cold frontal zone. The positive friction-induced height tendency over the surface low extends much higher than at 1200/19, but values in excess of 10 m (6 h)^{-1} are still restricted below 600 mb (Fig. 9c). In the cross section for diabatic heating (Fig. 9d), a vertical dipole is still visible, although this is less symmetric than at 1200/19: the marked increase in the negative height tendency in the lower troposphere is not accompanied by an increase in the positive height tendency aloft. Finally, the ageostrophic tendency term is still largest in the lowest troposphere (Fig. 9e).

e. Direct and indirect effects of vorticity advection and friction

At the end of section 2, several issues were listed that might be relevant in discussing the physical interpretation of the height tendencies calculated with the present method. As the first of these issues, the direct and indirect effects of vorticity advection and friction are addressed. The direct effect denotes here the height tendency obtained by substituting to (7) the vorticity tendency due to the first rhs term in (4) or (5). The indirect effect, in turn, refers to the height tendency attributable to the second, third, and fourth rhs terms in (4) or (5) that stem from the vertical motions induced by the direct forcing.

Figure 10 shows cross sections of the height tendencies induced directly and indirectly by vorticity advection at 1200/19 (above) and 0000/21 (below). In most of the vertical plane, the direct and the indirect effect are at both times seen to oppose each other. At 0000/21, they have the same sign between 500 and 900 mb near the western edge of the cross section, but this is a layer with a relatively small positive directly forced height tendency sandwiched between larger positive tendencies above and below. Thus, even in this case, the indirect effect acts to smooth out the vertical gradients in the height tendency distribution. With the exception of the lowest troposphere where the direct and the indirect effect have a comparable magnitude, the former generally dominates over the latter.

The substantial negative and positive directly forced height tendencies at the two sides of the upper trough are hardly a surprising finding. What may deserve more attention is the extended area of height increase that the direct effect at both times yields in the lowest tropo-

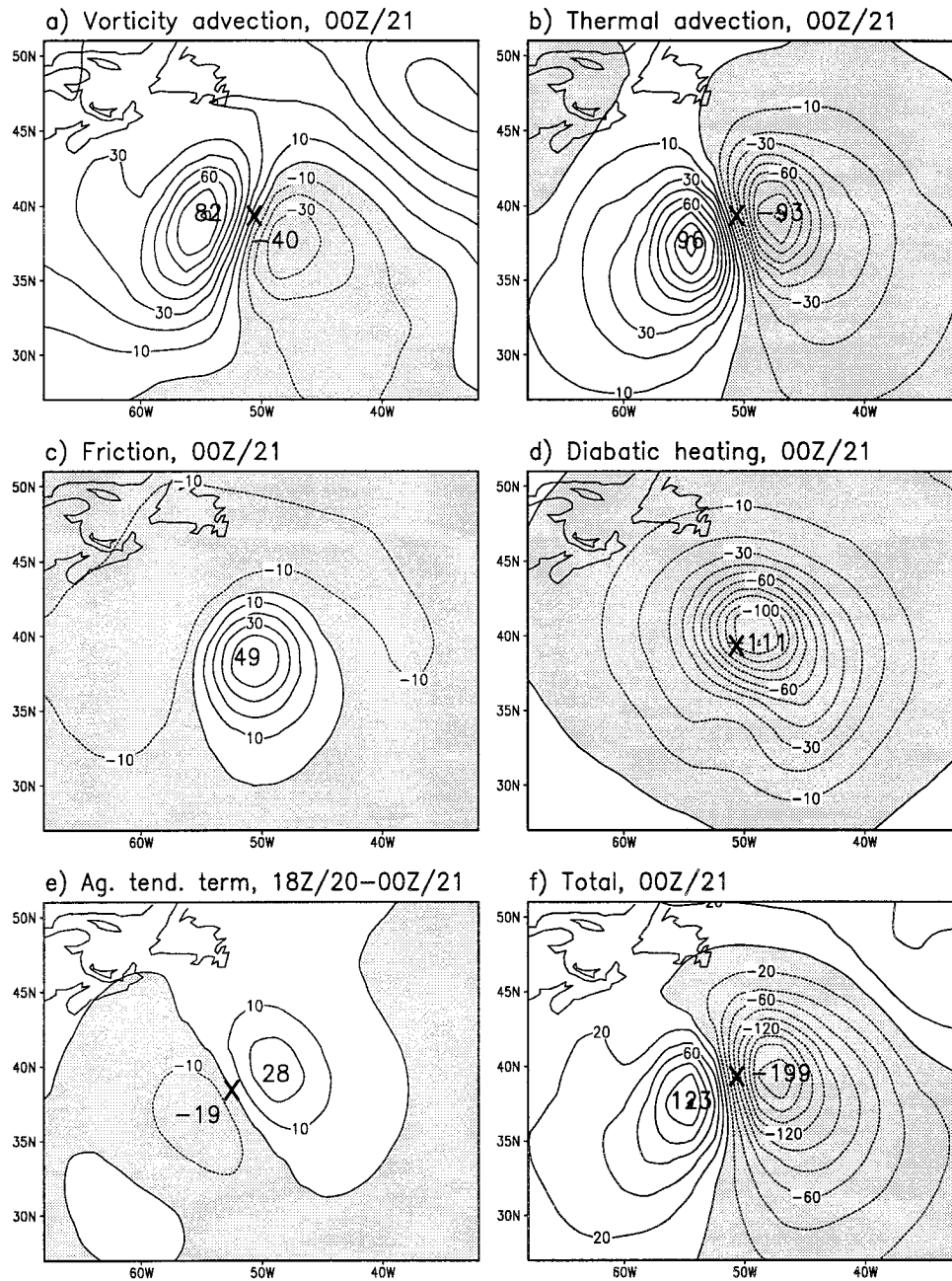


FIG. 8. As Fig. 6 but height tendencies at 0000 UTC 21 February [(a), (b), (c), (d), and (f)] or between 1800 UTC 20 February and 0000 UTC 21 February 1979 (e).

sphere. As discussed in the following subsection, this widespread (and particularly at 0000/21 very large) positive directly forced height tendency results from anticyclonic vorticity advection by low-level convergent winds.

Analogous to Fig. 10, the height tendencies induced directly and indirectly by friction at 0000/21 are shown in Fig. 11; 1200/19, when the cyclone was weaker, is excluded for brevity. The direct effect (Fig. 11a) is large

in the lowest troposphere [over 200 m $(6 \text{ h})^{-1}$ near the center of the low] but negligible above 800 mb. The indirect effect (Fig. 11b) strongly opposes the direct effect at the lowest levels, but it changes sign between 875 and 825 mb and remains positive over the surface low up to 325 mb. Thus, Figs. 11a and 11b, together with their sum in Fig. 9c, provide a nice demonstration of the concept of Ekman pumping discussed, for instance, by Holton (1992, 133–139).

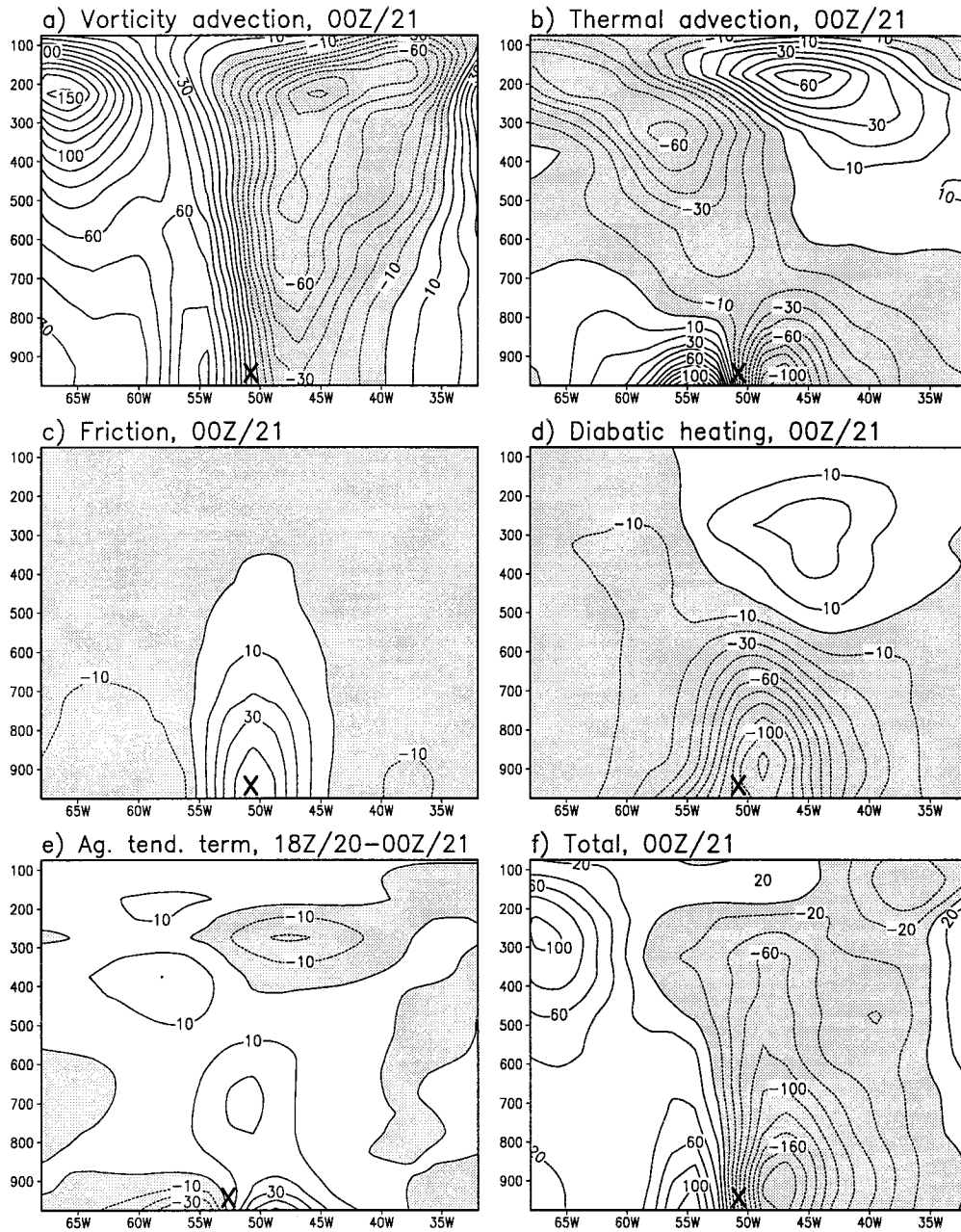


FIG. 9. As Fig. 8 but cross sections along 39.4°N.

f. Contributions of vorticity and thermal advection by nondivergent and divergent winds

As discussed in section 2, some of the terms formally treated as forcing in the present diagnostic system are in fact physically connected to the distribution of vertical motions. The most unambiguous examples are vorticity advection and thermal advection by divergent wind. To study the significance of this issue, the advections by the nondivergent (\mathbf{V}_ψ) and the divergent (\mathbf{V}_χ) winds were calculated separately. Their individual vor-

ticity tendency contributions were then computed from, for example,

$$\left(\frac{\partial \zeta}{\partial t}\right)_{V_\chi} = -\mathbf{V}_\chi \cdot \nabla(\zeta + f) - \omega_{V_\chi} \frac{\partial \zeta}{\partial p} + (\zeta + f) \frac{\partial \omega_{V_\chi}}{\partial p} + \mathbf{k} \cdot \left(\frac{\partial \mathbf{V}}{\partial p} \times \nabla \omega_{V_\chi}\right), \quad (10)$$

where ω_{V_χ} denotes the vertical motion obtained by forc-

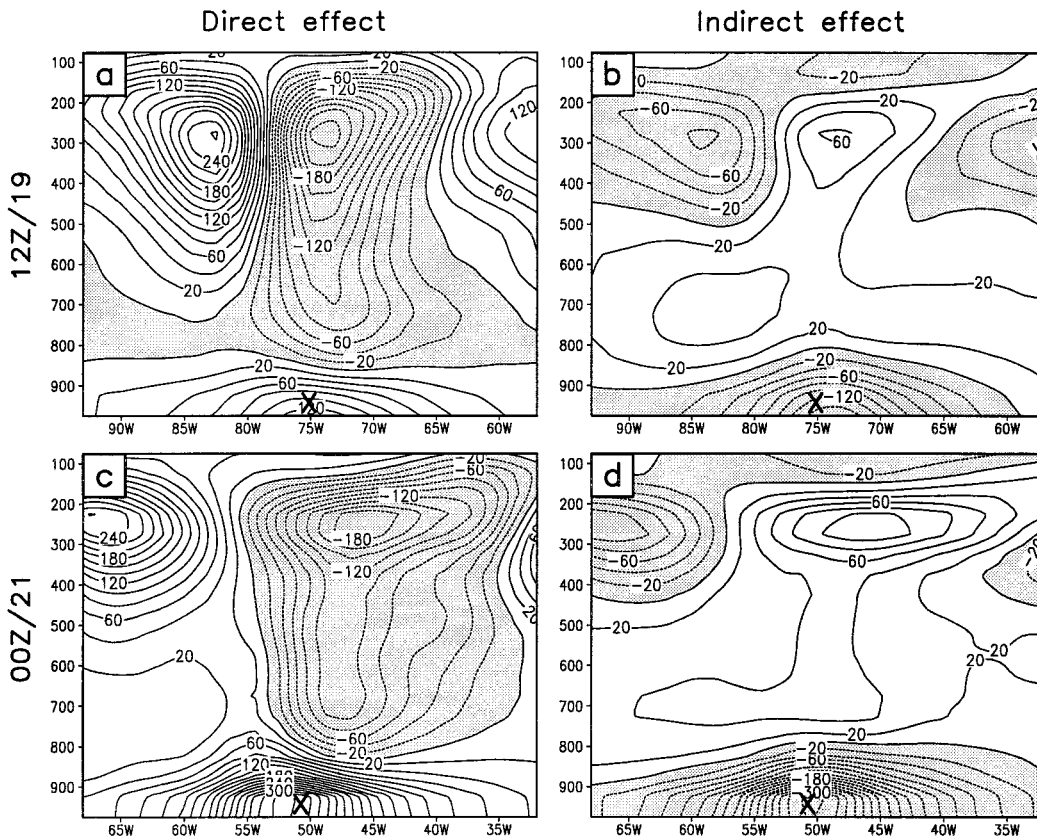


FIG. 10. Height tendencies induced directly [(a) and (c)] and indirectly [(b) and (d)] by vorticity advection. The cross sections in (a) and (b) are from 37.5°N at 1200 UTC 19 February and those in (c) and (d) from 39.4°N at 0000 UTC 21 February 1979. Contour interval is 20 m (6 h)⁻¹; negative values are shaded. The sum of (a) and (b) is shown in Fig. 7a and that of (c) and (d) in Fig. 9a.

ing (1) with $-\mathbf{V}_x \cdot \nabla(\zeta + f)$, and the corresponding height tendencies were estimated from (7).

The most interesting finding from this exercise was that vorticity advection by \mathbf{V}_x induced a widespread positive height tendency around the surface low (see Figs. 12b and 12d). This positive height tendency was

much stronger at 0000/21 than at 1200/19, and it maximized at both times in the lowest troposphere. Although this height tendency was largest somewhat to the west of the low center, especially at 0000/21, this mechanism in fact appears to be as important a brake for the development of the low-level cyclone as surface friction

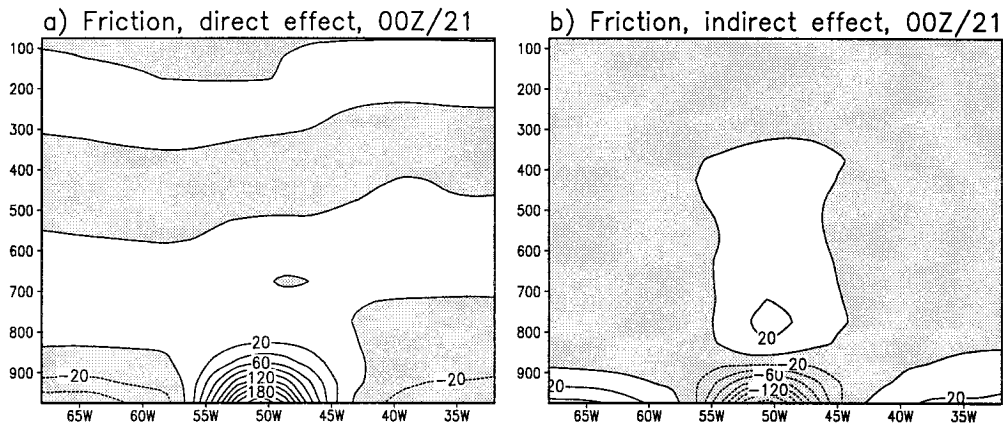


FIG. 11. Height tendencies induced (a) directly and (b) indirectly by friction at 39.4°N at 0000 UTC 21 February 1979. Contour interval is 20 m (6 h)⁻¹; negative values are shaded. The sum of (a) and (b) is shown in Fig. 9c.

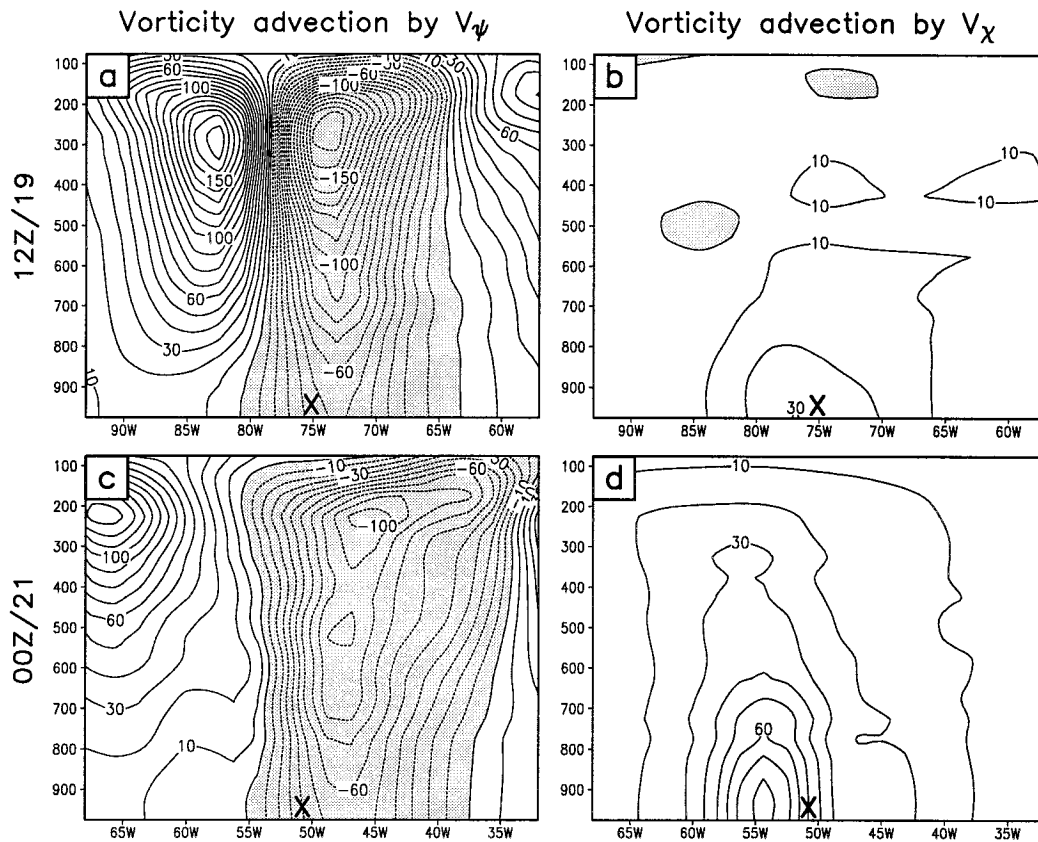


FIG. 12. Height tendencies due to vorticity advection by nondivergent [(a) and (c)] and divergent wind [(b) and (d)]. (a) and (b) are cross sections along 37.5°N at 1200 UTC 19 February and (c) and (d) cross sections along 39.4°N at 0000 UTC 21 February 1979. Contour interval is 10 m (6 h)^{-1} ; negative values are shaded. The sum of (a) and (b) is shown in Fig. 7a and that of (c) and (d) in Fig. 9a.

(compare Figs. 12b and 12d with Figs. 7c and 9c). This importance is a seemingly new finding. Although Hoskins and Sardeshmukh (1987) showed that vorticity advection by \mathbf{V}_x plays a significant role in the planetary

scale, this process appears to have received little attention in earlier synoptic-scale studies.

To investigate the role of vorticity advection by \mathbf{V}_x in more depth, a division to the directly and indirectly forced height tendencies was made in the manner described in section 5e. The direct effect was strongest in the lowest troposphere; above 800 mb it was actually very weak. The explanation for this strong low-level effect contains two factors that were already qualitatively valid at 1200/19 but were more conspicuous at 0000/21 (see Fig. 13). First, there was a very steep vorticity gradient between the surrounding anticyclonic areas and the center of the low. Second, in accord with the presence of an intense maximum of midtropospheric ascent just to the northeast of the center of the low, \mathbf{V}_x was generally directed across this gradient toward the core area of the cyclone. It also had a substantial magnitude, approaching 15 m s^{-1} in some areas at 0000/21. Together, these factors yielded a wide area of predominantly anticyclonic low-level vorticity advection.

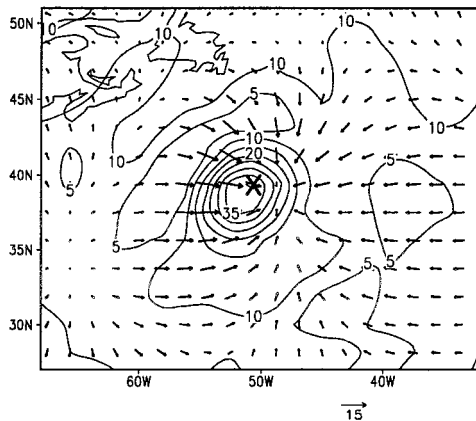


FIG. 13. Divergent wind (vector scale in meters per second) and absolute vorticity (contours every $5 \times 10^{-5} \text{ s}^{-1}$) at 950 mb at 0000 UTC 21 February 1979.

The discussion above is not to imply that vorticity advection by \mathbf{V}_ψ would have been insignificant. This component created by far the dominant part of $(\partial z/\partial t)_v$

in the mid- and upper troposphere, and it actually played an important role in the lowest troposphere as well (see Figs. 12a and 12c). By inducing an appreciable negative low-level height tendency over and to the east of the low, vorticity advection by \mathbf{V}_ψ favored the deepening of the surface low at both 1200/19 and 0000/21. Since the direct effect of vorticity advection by \mathbf{V}_ψ was small below 850 mb, these low-level height decreases must have been indirectly forced by advection in the mid- and upper troposphere.

In contrast with the case of vorticity advection, thermal advection by \mathbf{V}_χ was found to be of little importance. Apart from slightly enhancing the height increase in the very lowest troposphere at the western side of the low at 0000/21, this component was negligible compared with thermal advection by \mathbf{V}_ψ .

g. Calculations with a simplified equation system

The system consisting of the generalized omega equation (1), the complete vorticity equation (2), and the time derivative of the NLBE (7) contains several coefficients that vary rapidly in space and time. The lhs operator of (1) is dependent on the three-dimensional distributions of hydrostatic stability and absolute vorticity and on the vertical wind shear. Similarly, the vorticity and wind distributions enter as coefficients in the terms containing ω in (2). Finally, by determining the spatial derivatives of the streamfunction, the vorticity distribution affects the second rhs term of (7). Therefore, the height tendencies calculated with this system are not determined by the forcing (given by vorticity advection, thermal advection, friction, diabatic heating, and the ageostrophic tendency term) alone but are also affected by the environment that controls the various nonconstant coefficients. To demonstrate this, we use in this subsection a simpler equation system that retains the same forcing as our full system but by excluding some terms in converting the forcing into height tendencies largely eliminates the influence of the environmental variations. The generalized omega equation is replaced with

$$\sigma_0(p)\nabla^2\omega + f^2\frac{\partial^2\omega}{\partial p^2} = F_V + F_T + F_F + F_Q + F_A, \tag{11}$$

where $\sigma_0(p)$ denotes the global isobaric average of σ . In accord with this change, vertical vorticity advection, the tilting term, and the term $\zeta(\partial\omega/\partial p)$ are removed from the vorticity equation:

$$\frac{\partial\zeta}{\partial t} = -\mathbf{V}\cdot\nabla(\zeta + f) + f\frac{\partial\omega}{\partial p} + \mathbf{k}\cdot\nabla \times \mathbf{F}. \tag{12}$$

Finally, the NLBE is replaced with the linear balance equation

$$g\nabla^2\frac{\partial z}{\partial t} = \nabla\cdot\left(f\nabla\frac{\partial\psi}{\partial t}\right). \tag{13}$$

Thus, the variability of coefficients is fully eliminated apart from the slow meridional variation of the Coriolis parameter and the average vertical variation of the hydrostatic stability.

The total 925-mb height tendencies calculated with the simplified system are shown in Figs. 14a (1200/19) and 14b (0000/21). The differences from the solution of the full system (Figs. 6f and 8f) are considerable. At both times, the simplified system yields a somewhat looser couplet of height decrease and height increase and the maximum height decrease ahead of the low is substantially smaller. The height increase at the rear side of the low is less severely affected; it is somewhat larger at 1200/19 and slightly smaller at 0000/21. Consequently, the simplified system captures the rapid deepening of the low at 1200/19 much less well than the full system. At 0000/21, the cyclone was only slowly deepening according to the FGGE analyses, so the modest weakening implied by the simplified system is not more unreasonable than the marked deepening implied by the full system. As far as the overall magnitude and spatial structure of the height tendencies are considered, however, the solution of the simplified system is even at this time the less realistic of the two. One might argue that this is because this system is internally inconsistent, that is, the forcing derives from the primitive equations but the methods used in calculating the response follow the QG approximations (apart from that the variation of the Coriolis parameter is fully included). However, replacing the full forcing in this system with the QG counterpart (that is, vorticity advection and temperature advection calculated from the geostrophic assumption) yielded equally unrealistic results (Figs. 14c,d).

To analyze the factors that created differences between the full and the simplified solution, a number of sensitivity experiments were made. These addressed, in turn, the horizontal stability variations in the omega equation, the differences between the full vorticity equation and (12) (considered together with the corresponding lhs terms in the omega equation), and the nonlinear term in the NLBE. Although the effect of stability variations was not found to be negligible, the majority of the differences between the full and the simplified solution appeared to be associated with the strong low-level cyclonic vorticity.

To some extent, the impact of the vorticity distribution was simply associated with the nonlinear term in the NLBE. By including this term, the NLBE approximately accounts for the subgeostrophy of cyclonally curved flow in gradient wind balance and hence yields, for a given field of vorticity tendencies, larger height tendencies in cyclonic than anticyclonic areas. At 0000/21, both the maximum negative and positive height tendencies were increased by roughly 50%.

However, the strong low-level cyclonic vorticity also affected the calculated vorticity tendencies and did this in a way that favored height decreases at the expense of height increases. As the net result of two conflicting

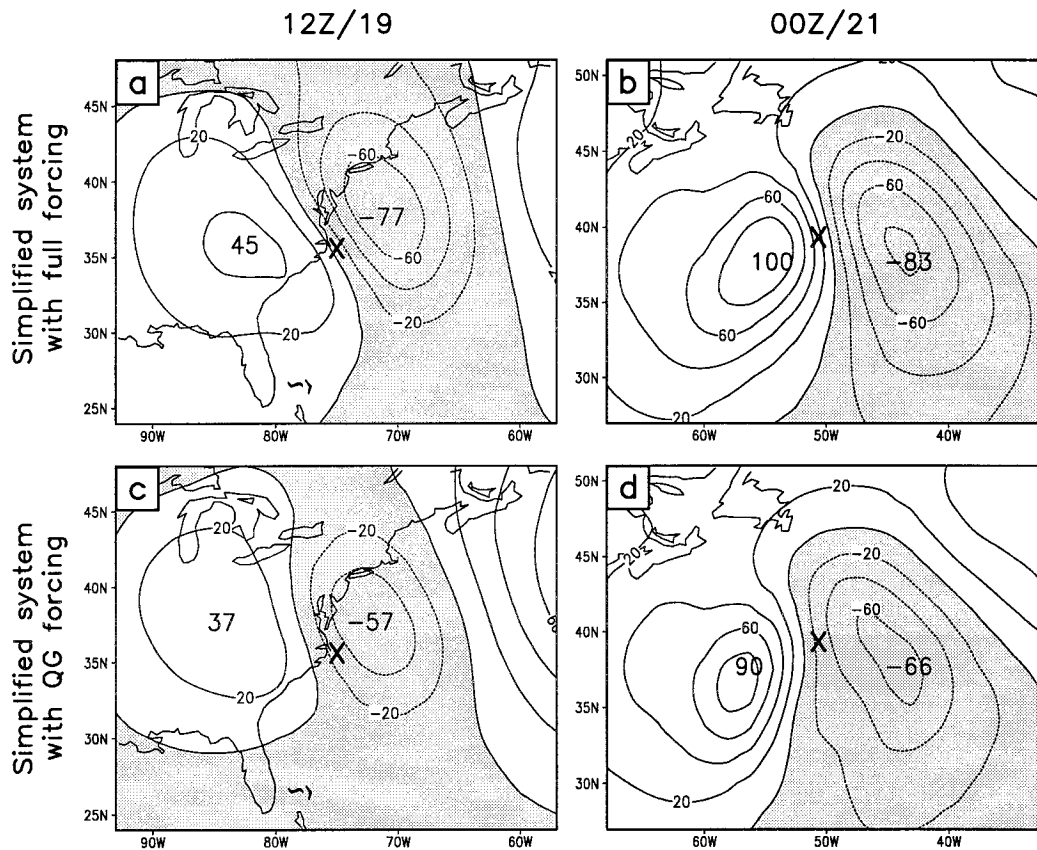


FIG. 14. Total height tendencies at 925 mb at (a) 1200 UTC 19 February and (b) 0000 UTC 21 February 1979 as calculated with the simplified system [Eqs. (11)–(13)]. Panels (c) and (d) are as (a) and (b) but the forcing includes only vorticity and temperature advection evaluated by using the geostrophic assumption. Contour interval is 20 m (6 h)⁻¹; negative values are shaded. The height tendencies obtained with the full system are shown in Figs. 6f and 8f.

factors, it enhanced the vorticity generation by the stretching mechanism in the area of low-level convergence over and to the east of the low center. On one hand, the term $\zeta(\partial\omega/\partial p)$ in (2) was large and positive. On the other hand, calculations with the omega equation indicated that [in accord with the findings of Pauley and Nieman (1992) for the *QE II* cyclone] the cyclonic vorticity acted to suppress the ascent especially below 800 mb, thereby weakening the convergence itself. The former factor was dominant, but the latter appeared to compensate roughly one-half of its influence.

In addition to producing different total height tendencies than the full system, the simplified system yielded a somewhat different picture of the roles of the individual forcing terms. For a striking example of this, the contributions of thermal advection and diabatic heating in this system are shown in Fig. 15. As found in sections 5c,d, there were important changes in these terms between 1200/19 and 0000/21 in the full system: thermal advection strongly promoted the deepening of the surface low at the former time but only acted to move the cyclone at the latter, and there was a large simultaneous increase in the negative height tendency

due to diabatic heating. In the simplified system, the changes from 1200/19 to 0000/21 are qualitatively similar but substantially less pronounced.

A clear though not unexpected indication of this comparison between the simplified system (with both the full and the QG forcing) and the full system is that, in analyzing intense or rapidly developing cyclones, approximate diagnostic techniques may be quantitatively quite inadequate. At least in general terms, in addition, the results serve to demonstrate that the height tendency response to a given forcing may be rather sensitive to the properties of the environment. In regard to the specific implications for the development of the Presidents' Day cyclone, however, one must be careful. For example, a tempting conclusion one might like to make is that the strong low-level cyclonic vorticity made the height tendencies near the center of the surface low more negative at both 1200/19 and 0000/21 and thus accelerated the explosive development of the storm and aided to prolong its subsequent slower deepening. This reasoning may well be qualitatively correct at least as far as the period of rapid deepening is concerned; the role of the low-level cyclonic vorticity in accelerating the

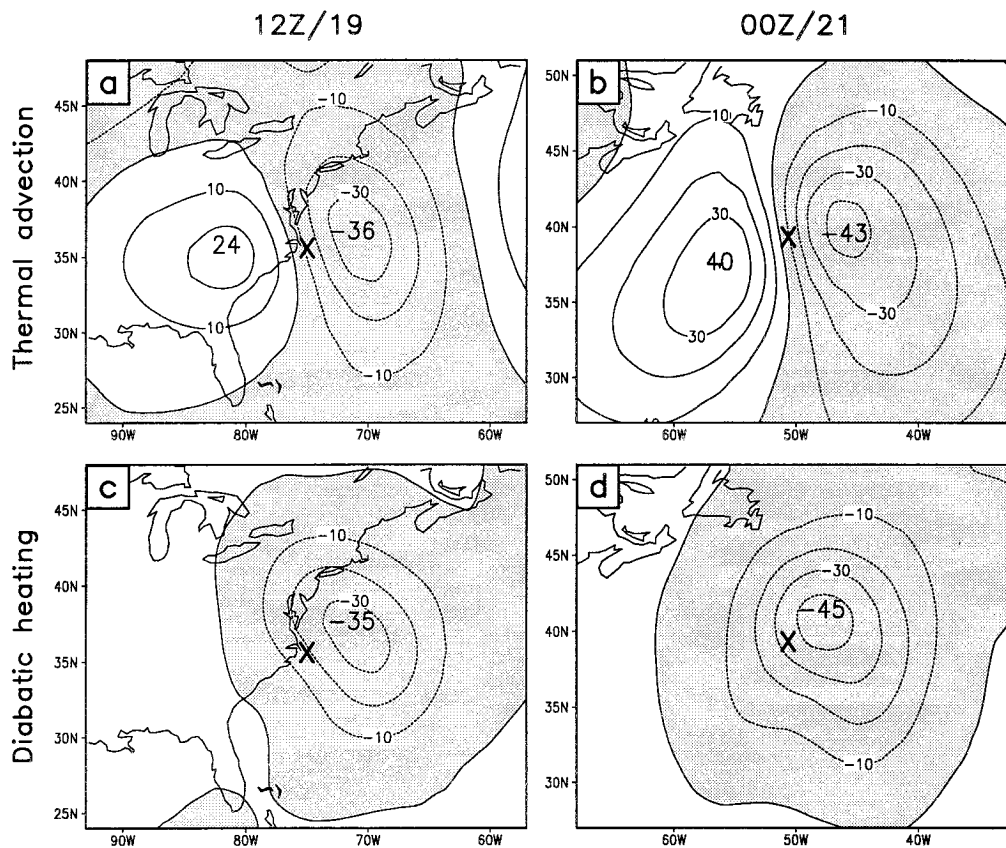


FIG. 15. Contributions of thermal advection [(a) and (b)] and diabatic heating [(c) and (d)] to height tendencies at 925 mb as calculated with the simplified system. Contour interval is 10 m (6 h)⁻¹; negative values are shaded.

rapid development in this particular case was also emphasized by Bosart and Lin (1984), and further support to this idea is provided by the more general study of Gyakum et al. (1992). However, the important complication that must be stressed is that the forcing and the environment are not rigorously independent from each other. In particular, if the low-level cyclonic vorticity had been weaker or absent, two important damping mechanisms would necessarily have been less efficient. With no significant low-level vorticity gradients, the strong negative vorticity advection by \mathbf{V}_x could not have existed. Likewise, if there had been no cyclonal low-level circulation, friction would not have acted to destroy it.

6. Summary and discussion

Height tendency dynamics were studied with a system consisting of three equations. By using a generalized omega equation and the vorticity equation, five components of vorticity tendency were first computed. The components due to vorticity advection and friction included both the vorticity tendency directly created by these processes and the indirect contribution from the vertical motions induced by them, while the other three (attributable to thermal advection, diabatic heating, and an ageostroph-

ic tendency term) only consisted of the indirect contribution. The corresponding five height tendency components were estimated by substituting the vorticity tendency components to a nonlinear balance equation.

The system was applied to an analysis of the Presidents' Day cyclone in February 1979, with the main focus on two synoptic times, one (1200/19) during the explosive development and the other (0000/21) during the maturity of the cyclone. A large part of the rapid deepening of the low-level cyclone at 1200/19 was found to be attributable to thermal advection and diabatic heating, which were of roughly equal importance. At 0000/21, thermal advection only appeared to propagate the cyclone, but in striking and perhaps surprising contrast, a much larger negative height tendency due to diabatic heating was actually found than at 1200/19.

The impact of vorticity advection was twofold: the advectons by the nondivergent (\mathbf{V}_ψ) and the divergent wind (\mathbf{V}_x) were found to play very different roles. The former made a significant contribution to deepen the surface low at both 1200/19 and 0000/21, but the latter acted to fill the low. Vorticity advection by \mathbf{V}_x was in fact found to be as important a damping mechanism for the low-level cyclone as surface friction, and, as in the case of friction, the positive height tendency induced

by it increased substantially from 1200/19 to 0000/21. The importance of this process is an interesting finding that seems to have been to some extent overlooked in earlier studies of cyclone dynamics. Obviously, however, this importance is also somewhat disturbing: although formally treated as such in the present diagnostic system, \mathbf{V}_x is not physically independent of ω . This actually inspires us to suggest a possible modification to the system (see the last paragraph of this text).

Some important insights were also gained by dividing the contributions of vorticity advection and friction into parts associated with the direct forcing and the indirect forcing due to the vertical motions induced. In particular, the efficiency of vertical motions in smoothing out the vertical gradients in the direct forcing was demonstrated.

Finally, it is clear that the present analysis has left many issues unresolved. The calculated height tendencies implied a somewhat too small deepening rate for the cyclone at 1200/19 and a too large deepening rate at 0000/21. While it is difficult to attribute these problems to any single factor, it cannot be ruled out, for example, that the model-produced diabatic heating at the latter time was to some extent too strong, resulting in an overestimate of the negative height tendency induced by this term. Likewise, the large differences between the results of the simplified equation system in section 5g and those of the full system do raise some questions. The basic implication that cyclone development is not determined by the strength of the forcing alone but may as much depend on a suitable environment is, although in agreement with earlier research (e.g., Reed 1990; Uccellini 1990; Gyakum et al. 1992), somewhat disappointing for anyone yearning for simple explanations. At the same time, these differences serve to remind us that the conclusions one obtains from height tendency calculations may be sensitive to relatively subtle details in the methodology. In this context, it is good to recall that the present approach for eliminating vertical motions as an independent forcing agent is not unique. As noted in section 2, one could also proceed, after solving the generalized omega equation, by using the thermodynamic equation approach of Hirschberg and Fritsch (1991) or the Tsou et al. (1987) height tendency equation. Whether these choices would lead to significantly different diagnostics is an obvious issue for further study.

Another suggestion for future studies concerns the advections by the divergent wind. In the present study, these were formally treated as independent forcing mechanisms, neglecting the inherent physical dependence of \mathbf{V}_x from ω via the continuity equation. Had it been found that vorticity and temperature advection by \mathbf{V}_x would both have been unimportant, this neglect would be of little concern. However, as this was clearly not the case, the following procedure might be worth considering in future studies, even though this would complicate the calculations. It would be possible to reformulate the diagnostic system so that the direct advective forcing in the omega and vorticity equations

would only contain the advections by \mathbf{V}_ψ . Vorticity and temperature advection by \mathbf{V}_x would be moved to the lhs of the omega equation and \mathbf{V}_x would be solved simultaneously with ω in the way discussed by Krishnamurti (1968). In the vorticity equation, vorticity advection by \mathbf{V}_x would then be treated as part of the indirect forcing. Since the system would still be linear with respect to the quantities solved [at least if we neglect in $L(\omega)$ and in the vorticity equation the dependence of $\partial\mathbf{V}/\partial p$ from \mathbf{V}_x], a division of $\partial z/\partial t$ into five parts would still be obtained. Now, however, the first two parts would be associated with vorticity and temperature advection by \mathbf{V}_ψ rather than with the advections by the total wind. In this way, the important but physically unimportant contribution of vorticity advection by \mathbf{V}_x would be divided between other processes.

Acknowledgments. The basic idea of this study originates from a discussion with Melvyn A. Shapiro during his visit to Helsinki in September 1993. Other persons specially acknowledged are Klaus Arpe and Sakari Uppala for providing the ECMWF data and Eero Holopainen and the anonymous reviewers for their comments on the manuscript. The author of the study is presently financed by the Academy of Finland.

REFERENCES

- Bosart, L. F., 1981: The Presidents' Day snowstorm of 18–19 February 1979: A subsynoptic-scale event. *Mon. Wea. Rev.*, **109**, 1542–1566.
- , and S. C. Lin, 1984: A diagnostic analysis of the Presidents' Day storm of February 1979. *Mon. Wea. Rev.*, **112**, 2148–2177.
- Charney, J., 1955: The use of the primitive equations of motion in numerical prediction. *Tellus*, **7**, 22–26.
- Davis, C. A., E. D. Grell, and M. A. Shapiro, 1996: The balanced dynamical nature of a rapidly intensifying oceanic cyclone. *Mon. Wea. Rev.*, **124**, 3–26.
- Gyakum, J. R., P. J. Roebber, and T. A. Bullock, 1992: The role of antecedent surface vorticity development as a conditioning process in explosive cyclone intensification. *Mon. Wea. Rev.*, **120**, 1465–1489.
- Haltiner, J. G., and R. T. Williams, 1980: *Numerical Prediction and Dynamic Meteorology*. Wiley and Sons, 477 pp.
- Hirschberg, P. A., and J. M. Fritsch, 1991: Tropopause undulations and the development of extratropical cyclones. Part II: Diagnostic analysis and conceptual model. *Mon. Wea. Rev.*, **119**, 518–550.
- Holton, J. R., 1992: *An Introduction to Dynamic Meteorology*. 3d ed. Academic Press, 511 pp.
- Hoskins, B. J., and P. D. Sardeshmukh, 1987: Transient eddies and the seasonal mean rotational flow. *J. Atmos. Sci.*, **44**, 328–338.
- Krishnamurti, T. N., 1968: A diagnostic balance model for studies of weather systems of low and high latitudes, Rossby number less than 1. *Mon. Wea. Rev.*, **96**, 197–207.
- Pauley, P. M., and S. J. Nieman, 1992: A comparison of quasigeostrophic and nonquasigeostrophic vertical motions for a rapidly intensifying marine extratropical cyclone. *Mon. Wea. Rev.*, **120**, 1108–1134.
- Räisänen, J., 1995: Factors affecting synoptic-scale vertical motions: A statistical study using a generalized omega equation. *Mon. Wea. Rev.*, **123**, 2447–2460.
- Reed, R. J., 1990: Advances in knowledge and understanding of extratropical cyclones during the past quarter century: An over-

- view. *Extratropical Cyclones. The Erik Palmen Memorial Volume*, C. Newton and E. O. Holopainen, Eds., Amer. Meteor. Soc., 27–45.
- Tan, Y.-C., and J. A. Curry, 1993: A diagnostic study of the evolution of an intense North American anticyclone during winter 1989. *Mon. Wea. Rev.*, **121**, 961–975.
- Tsou, C.-H., and P. J. Smith, 1990: The role of synoptic/planetary-scale interactions during the development of a blocking anticyclone. *Tellus*, **42A**, 174–193.
- , —, and P. M. Pauley, 1987: A comparison of adiabatic and diabatic forcing in an intense extratropical cyclone system. *Mon. Wea. Rev.*, **115**, 763–786.
- Uccellini, L. W., 1990: Processes contributing to the rapid development of extratropical cyclones. *Extratropical Cyclones. The Erik Palmen Memorial Volume*, C. Newton and E. O. Holopainen, Eds., Amer. Meteor. Soc., 81–105.
- , P. J. Kocin, R. A. Petersen, C. H. Wash, and K. F. Brill, 1984: The Presidents' Day cyclone of 18–19 February 1979: Synoptic overview and analysis of the subtropical jet streak influencing the pre-cyclogenetic period. *Mon. Wea. Rev.*, **112**, 31–55.
- , D. Keyser, K. F. Brill, and C. H. Wash, 1985: The Presidents' Day cyclone of 18–19 February 1979: Influence of upstream trough amplification and associated tropopause folding on rapid cyclogenesis. *Mon. Wea. Rev.*, **113**, 962–988.
- , R. A. Petersen, K. F. Brill, P. J. Kocin, and J. Tuccillo, 1987: Synergistic interactions between an upper-level jet streak and diabatic processes that influence the development of a low-level jet and a secondary coastal cyclone. *Mon. Wea. Rev.*, **115**, 2227–2261.
- Wergen, W., 1988: The diabatic ECMWF normal mode initialisation scheme. *Beitr. Phys. Atmos.*, **61**, 274–302.
- Whitaker, J. S., L. W. Uccellini, and K. F. Brill, 1988: A model-based diagnostic study of the rapid development phase of the Presidents' Day cyclone. *Mon. Wea. Rev.*, **116**, 2337–2365.